Korean J. Chem. Eng., 39(3), 798-810 (2022)
DOI: 10.1007/s11814-021-0943-9

pISSN: 0256-1115
eISSN: 1975-7220

Molecular weight distribution modeling of LDPE in a continuous stirred-tank reactor using coupled deterministic and stochastic approach

Solji Choi, Yongkyu Lee, Seongho Park, and Jong Min Lee†

School of Chemical and Biological Engineering, Seoul National University, Seoul 08826, Korea
(*Received 11 May 2021 • Revised 22 August 2021 • Accepted 26 August 2021*)

Abstract−A hybrid approach that combines the method of moments and Monte Carlo simulation to predict the molecular weight distribution of low-density polyethylene for a continuous stirred tank reactor system is proposed. A 'Block', which is repeating reaction group, is introduced for the calculation cost-effective simulation. This model called the 'block Kinetic Monte Carlo' is ~10 to 32 times faster than Neuhaus's model. The model can be applied to any steady state system and provide a calculation cost reduction effect, where one reaction is much faster than others, for example, the propagation reaction. Furthermore, we performed a case study on the effects of the system temperature and initiator concentration on the MWD and reaction rate ratio. Based on the simulation results of 180 case studies, we determined a quantitative guideline for the appearance of shoulder, which is a function of the rate ratio of reactions to the propagation reaction.

Keywords: Molecular Weight Distribution, LDPE, CSTR, Hybrid Model, Method of Moment, Kinetic Monte Carlo

INTRODUCTION

Low-density polyethylene (LDPE) is produced under a high-pressure by free-radical polymerization. Unlike high-density polyethylene (HDPE), which has scarce branching, LDPE has high-density long-chain branches owing to the scission and chain transfer reactions. Because of its features, LDPE has a low tensile strength and high ductility, which improves flexibility and transparency. Therefore, LDPE can form various shapes and produce most films and plastic bags.

There are several factors that represent the physical properties of polymers, such as number average molecular weight (Mn), weight average molecular weight (Mw), melt index (MI), molecular weight distribution (MWD), and polydispersity index (PDI). Other properties only represent the average value, whereas MWD shows the weight ratio of each polymer component. The shape of the MWD allows us to predict polymer processability and product quality. For example, a narrow MWD enhances polymer quality and a wide MWD allows for easier processing. The shoulders and tails of the MWD contain information about the density of chain branching. Short chain branching reduces the density of polymer [1], and long-chain branching increases the sensitivity of melt viscosity [2]. To produce a polymer with the desired physical properties and improve the process productivity, an MWD prediction model is essential.

Many studies have been conducted to predict the MWD. MoM is the most popular method for predicting the average molecular weight [3-6]. MoM has been widely used in many studies to develop kinetic models for conventional free radical polymerization, coordination polymerization and others for linear and branched polymers [7-11]. One of the main advantages of this method is that it simplifies the theoretically infinite number of mass balance equations of chain species into a much smaller number of equations. In this method, only the average properties of the polymer can be calculated by ignoring the information about individual chains for simplification. By dividing an entire range of molecular weights into a limited number of intervals, the method of moments is capable of predicting molecular-weight distributions [12]. However, a large number of moments are required to obtain detailed information on MWD. Well and Ray segregated the polymer distribution into a large number of 'segments,' so that the model can predict the detailed shape of MWD and reveal the kinetic effects for the existence of MWD shoulder [12]. Because the model requires a minimum of 75 segments, at least 400 variables should be considered, which makes it difficult to find a solution. Another approach suggested by Pladis and Kiparissides is based on the 'classes,' in which the total polymer population is discretized according to the number of branches [13]. They assumed that the distribution of classes followed a log-normal distribution, which is not justified. In addition, MoM cannot explicitly implement scission. In an environment where the production conditions exceed 300 °C, chain scission becomes dominant owing to the high-temperature sensitivity [14]. Because the molecules split differently depending on their topology, moments including scission points must be introduced to simulate the scission. In this case, the number of moments increases exponentially, making the problem difficult to solve. Therefore, in most studies on MoM, a random scission mechanism that does not require the chain topology information has been adopted. In addition, the MoM model requires a closure relationship assumption [10] to solve the scission. The model error accumulates due to the ambiguous implementation of the chain scission.

In contrast to MoM, the Monte Carlo (MC) technique can accurately implement scission based on the topological information.

†To whom correspondence should be addressed.
E-mail: jongmin@snu.ac.kr

Numerous studies have been conducted to investigate the effect of chain scission on the physical properties of polymers using the MC technique [16-24]. Gillespie proposed the Kinetic Monte Carlo (KMC) algorithm, which has been applied to many other studies [25]. However, this method cannot be directly applied to continuous reactors, in which chains with different residence times exist. Tobita first proposed an individually branched polymer chain methodology [26]. He introduced the concept of a primary chain to which all branch points are connected and assumed that the primary chain is severed [26]. It can simulate chains with different residence times and predict the MWD in various types of reactors, such as continuous stirred tank reactors (CSTRs), tubular reactors, and tanks-in-series reactors [27,28]. However, this approach requires prior knowledge of the branch density and segment length following the Flory distribution [29]. Moreover, MC simulation has an issue of exorbitant computational time, which is not suitable for industrial applications.

Studies have been conducted to reduce the computation time by combining deterministic methods with stochastic techniques [18,30-32]. Meimaroglou proposed a kinetic/topology MC algorithm for a multizonal tubular reactor [18]. The topological information of the macromolecule was obtained by the MC algorithm with the kinetic model of the tubular reactor. This method does not require any assumptions about the distribution of live and dead polymers, but the model cannot be extended to CSTR because all macromolecules have the same residence time [33]. Neuhaus developed a hybrid model that coupled deterministic and stochastic approaches that could be applied to the tubular and autoclave reactors [32]. The single macromolecule approach (SMMA) introduced in the model allows the parallel computation of large molecule ensembles and reduces the computation time efficiently. In Eckes's study [32], polymer chains that are combined with the macromolecules via termination by combination are sampled from the previously stored chain data. Although this approach is valid for tubular reactors, it encounters a recursion in the CSTR reactor. This is because the chain to be combined may have a longer residence time than the macromolecules. In addition, to achieve sufficient accuracy, ten million molecules must be simulated. This requires approximately one hour even with parallelized computation, which is not practical for industrial applications [30].

Both approaches have technical issues, such as MoM cannot implement the topological scission, and MC is computationally intensive. Therefore, this study proposes a hybrid model approach consisting of the MoM and KMC for a CSTR. The proposed model can implement scission, resolve recursion, and significantly reduce calculation time. The model is validated with the model proposed by Neuhaus [25] by comparing its performance and calculation time. In addition, we extensively explored the MWD under various operating conditions and analyzed the effect of each element reaction. Given this, we can determine the effect of each reaction mechanism on the existence of the shoulder in MWD.

METHODOLOGY

To simulate polymerization in a steady-state reactor, such as CSTR, we developed a model that combined MoM and KMC.

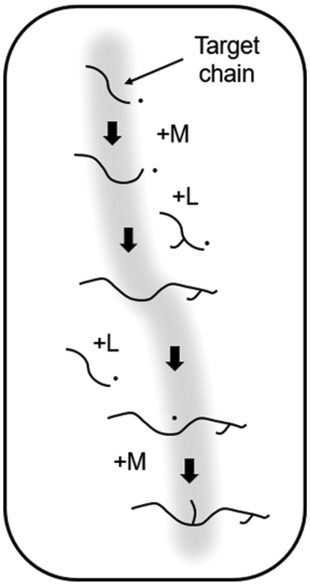

Fig. 1. Concept of target chain model.

Table 1. Elementary reactions of free radical polymerization

R_i	Initiation	$I \xrightarrow{f \cdot k_d} 2L_0$
$R_{p,1}$ $R_{p,2}$	Propagation	$L_m(L_{m,sec}) + M \xrightarrow{k_p} L_{m+1}$
R_t	Termination	$L_m + L_n \xrightarrow{k_t} D_{m+n}$
$R_{cp,1}$ $R_{cp,2}$	Chain transfer to polymer	$L_m + D_n \xrightarrow{k_{cp}} D_m + L_{n,sec}$
R_{cm}	Chain transfer to monomer	$L_m + M \xrightarrow{k_{cm}} D_m + L_0$
$R_{beta,1}$ $R_{beta,2}$	Beta scission	$L_{m,sec} \xrightarrow{k_{beta}} L_n + D_{m-n}$

First, the bulk polymer concentration was calculated using a mass balance and moment equation. Then, the detailed molecular weight distribution was derived using KMC. The newly proposed model is based on the 'single macromolecule approach' (SMMA) and we named the single macromolecule as 'target chain'. The concept of the target chain model is illustrated in Fig. 1.

1. Polymer Reaction Mechanism

LDPE is produced by free-radical polymerization, and the elementary reactions are presented in Table 1.

L_n represents a live polymer chain of length n, whose radical is located at the end of the chain. $L_{n,sec}$ represents a secondary radical polymer chain of length n, whose radical is located in the middle of the chain. Finally, D_n represents a dead polymer chain of length n. To avoid any confusion, we use different reaction names for the same class of reactions depending on the type of molecule that we track. In the case of the chain transfer to polymer, when the target chain is a live polymer, we name it $R_{cp,1}$ while the reaction is named $R_{cp,2}$ when the target chain is a dead polymer. In the case of the propagation reaction, when the target chain is a live polymer, we name it $R_{p,1}$ while the reaction is named $R_{p,2}$ when the target chain

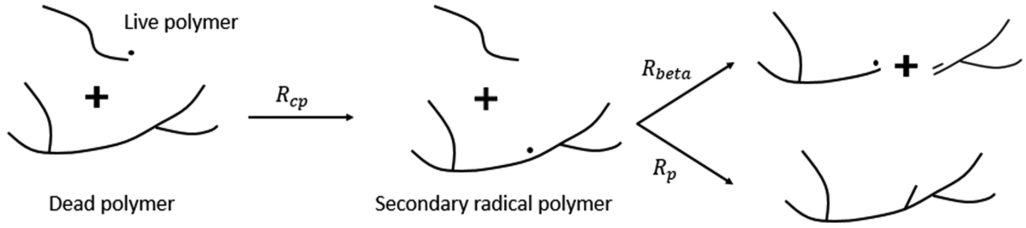

Fig. 2. Schematic of chain transfer to polymer reaction.

Table 2. Kinetic parameters of LDPE

$$k = A \cdot \exp\left(-\frac{E + P * \Delta V}{RT}\right)$$

	A (L/mol·s)	E/R (K)	ΔV (cm^3/mol)
k_d	$1.06 * 10^{16}$	17,972	2.5077
k_p	$1.14 * 10^{7}$	3,584	−19.7717
k_t	$3 * 10^{9}$	1,213	13.0443
k_{cp}	$2.92 * 10^{5}$	5,580	−20.06
k_{cm}	$1.67 * 10^{6}$	4,549	4.3937
k_{beta}	$1.04 * 10^{12}$	10,108	−19.27

is a secondary radical polymer. In the case of the beta scission, when the target chain formed after the reaction is a live polymer, we name it $R_{beta,1}$ while the reaction is named $R_{beta,2}$ when the chain formed after the reaction is a dead polymer. Sometimes, the chain transfer to solvent or chain transfer agent (CTA) and backbiting reactions are also involved in free radical polymerization [34]. However, the effect of the backbiting reaction on the molecular weight distribution is negligible [30], and the chain transfer to solvent or CTA has an effect similar to that of the chain transfer to the monomer. Therefore, these two reactions are not considered in this study. The most important reaction for LDPE to have high-density branches is the chain transfer to polymer. As shown in Fig. 2, a dead polymer becomes a secondary radical chain by obtaining a radical from a live polymer chain. Then, the propagation and beta scission occur sequentially in the secondary radical chain. When propagation occurs, the chain lengthens and forms long-chain branches. When beta scission occurs, the chain is split into two smaller molecules. Because of these two reactions, the MWD broadens. The beta scission includes two types of pathways: random scission and chain-end scission. Among these, the random scission is selected because it is more dominant in the simulated reaction. The kinetic parameters of each reaction are listed in Table 2.

2. Reactor Model

The most common reactor type for LDPE polymerization in industry, the autoclave reactor, is inappropriate for analysis with the proposed model because of the complex fluid dynamics and operation. Therefore, in this research, a model was developed in a series of CSTRs, each of which has one input and one output, and exhibits homogeneous temperatures and pressures. Because the autoclave reactor shows a similar behavior to the system composed of a series of CSTRs, the model can be extended to an autoclave reactor in practice.

The model consists of both deterministic and stochastic parts. In the deterministic part, the bulk polymer properties are calculated using MoM. Then, the calculated values are passed on to the stochastic part and are used to calculate the probability of each reaction. Based on these probabilities, the polymer chain length is determined stochastically using the MC technique.

3. Deterministic Part

The steady-state information of the polymer properties in CSTR can be calculated using a set of equations involving the momentum equation and mass balances. The equations for the initiator, monomer, live polymer, dead polymer, and secondary live polymer are presented below:

$$\frac{d[M]}{dt} = \frac{v}{V}[M]_{in} - k_p\lambda_0[M] - k_p\lambda_{sec,0}[M] - k_{cm}\lambda_0[M] - \frac{v}{V}[M] \quad (1)$$

$$\frac{d[I]}{dt} = \frac{v}{V}[I]_{in} - fk_d[I] - \frac{v}{V}[I] \quad (2)$$

$$\frac{d[L_n]}{dt} = \delta(n-1)(2fk_d[I] + k_{cm}\lambda_0[M]) - k_p([L_n] - [L_{n-1}] - [L_{sec,n}])[M] - k_t[L_n]\lambda_0 - k_{cp}[L_n]\mu_1 - k_{cm}[L_n][M] + k_{beta}\sum_{m=n+1}^{\infty}[\lambda_{sec,m}] - \frac{v}{V}[L_n] \quad (3)$$

$$\frac{d[D_n]}{dt} = k_t\sum_{m=1}^{n-1}[L_m][L_{n-m}] - k_{cp}\lambda_0 n[D_n] + k_{cp}[L_n]\mu_1 + k_{cm}[L_n][M] + k_{beta}\sum_{m=n+1}^{\infty}[\lambda_{sec,m}] - \frac{v}{V}[D_n] \quad (4)$$

$$\frac{d[L_{sec,n}]}{dt} = -k_p[L_{sec,n}][M] + k_{cp}\lambda_0 n[D_n] - k_{beta}[L_{sec,n}] - \frac{v}{V}[L_{sec,n}] \quad (5)$$

From these equations, the information on the polymer weight distribution is summed up with a couple of moments. From the definition of moment, the 0th, 1st, and 2nd moments of the live polymer, dead polymer, and secondary radical polymer are calculated as in Eqs. (6)-(8).

$$\lambda_k = \sum n^k[L_n] \quad (6)$$

$$\mu_k = \sum n^k[D_n] \quad (7)$$

$$\lambda_{sec,k} = \sum n^k[L_{sec,k}] \quad (8)$$

Each moment can be derived from Eqs. (1)-(8) with pseudo-steady state assumption, and the derived equations are given by:

$$\frac{d\lambda_0}{dt} = 2fk_d[I] + k_p\lambda_{sec,0}[M] - k_t\lambda_0^2 - k_{cp}\lambda_0\mu_1 + k_{beta}\lambda_{sec,0} - \frac{v}{V}\lambda_0 \quad (9)$$

$$\frac{d\lambda_1}{dt} = 2fk_d[I] + (k_{cm} + k_p)\lambda_0[M] - k_t\lambda_1\lambda_0 + k_p(\lambda_{sec,0} + \lambda_{sec,1}) - k_{cp}\lambda_1\mu_1 - k_{cm}\lambda_1[M] + k_{beta}\frac{(\lambda_0 + \lambda_1)}{2} - \frac{v}{V}\lambda_1 \quad (10)$$

$$\frac{d\lambda_2}{dt} = 2fk_d[I] + k_{cm}\lambda_0[M] + k_p[M](2\lambda_1 + \lambda_0) + k_p(\lambda_{sec,2} + 2\lambda_{sec,1} + \lambda_{sec,0})[M] - k_t\lambda_2\lambda_0 - k_{cp}\lambda_2\mu_1 - k_{cm}\lambda_2[M] + k_{beta}\frac{(2\lambda_2 + 3\lambda_1 + \lambda_0)}{6} - \frac{v}{V}\lambda_2 \quad (11)$$

$$\frac{d\mu_0}{dt} = \frac{k_t}{2}\lambda_0^2 + k_{cm}\lambda_0[M] + k_{beta}\lambda_{sec,0} - \frac{v}{V}\mu_0 \quad (12)$$

$$\frac{d\mu_1}{dt} = k_t(\lambda_0\lambda_1) - k_{cp}\mu_2\lambda_0 + k_{cp}\lambda_1\mu_1 + k_{cm}\lambda_1[M] + k_{beta}\frac{(\lambda_{sec,0} + \lambda_{sec,1})}{2} - \frac{v}{V}\mu_1 \quad (13)$$

$$\frac{d\mu_2}{dt} = k_t(\lambda_0\lambda_2 + \lambda_1^2) - k_{cp}\mu_3\lambda_0 + k_{cp}\lambda_2\mu_1 + k_{cm}\lambda_2[M] + k_{beta}\frac{(2\lambda_{sec,2} + 3\lambda_{sec,1} + \lambda_{sec,0})}{6} - \frac{v}{V}\mu_2 \quad (14)$$

$$\frac{d\lambda_{sec,0}}{dt} = -k_p\lambda_{sec,0}[M] + k_{cp}\lambda_0\mu_1 - k_{beta}\lambda_{sec,0} - \frac{v}{V}\lambda_{sec,0} \quad (15)$$

$$\frac{d\lambda_{sec,1}}{dt} = -k_p\lambda_{sec,1}[M] + k_{cp}\lambda_0\mu_2 - k_{beta}\lambda_{sec,1} - \frac{v}{V}\lambda_{sec,1} \quad (16)$$

$$\frac{d\lambda_{sec,2}}{dt} = -k_p\lambda_{sec,2}[M] + k_{cp}\lambda_0\mu_3 - k_{beta}\lambda_{sec,2} - \frac{v}{V}\lambda_{sec,2} \quad (17)$$

Given these equations, the problems cannot be closed because of μ_3. Therefore, μ_3 is obtained using the closure technique suggested by Zabisky [36].

$$\mu_3 = \left(\frac{\mu_2}{\mu_1}\right)^2\sqrt{2\mu_2\mu_0 - \mu_1^2} \quad (18)$$

4. Stochastic Part

We now introduce a new stochastic algorithm called 'Block KMC'. This method is based on the conventional KMC and dramatically reduces the calculation time by introducing the concept of 'Block'. Based on the steady-state assumption, each algorithm step can be simultaneously simulated in block units, and the calculation time can be reduced because the propagation reaction is dominant compared to other reaction components. The detailed algorithm is described in the following subsections.

4-1. KMC

The typical algorithm of KMC was proposed by Gillespie, and a flowchart is shown in Fig. 3 [25].

First, the stochastic rates are calculated based on the bulk polymer concentrations, and propensity functions are generated. Then, one reaction is selected with a random number between 0 and 1 based on these probabilities, and the state is updated with this reaction. Subsequently, the time is updated by marching forward over a single time interval. The simulation is repeated until the total time reaches the residence time.

It is difficult to directly apply this algorithm to our model because each polymer chain has a different residence time in the CSTR. Therefore, we employ the concept of a target chain and combine KMC with MoM. The detailed algorithm of the target chain model is shown in Fig. 4.

The residence time distribution in CSTR is known by the Eqs. (19)-(20) and residence time distribution according to the number of CSTR is shown in Fig. 5.

$$E(\theta) = \frac{1}{T}\exp(-\theta) \quad (19)$$

$$\theta = \frac{\tau}{T} \quad (20)$$

The stochastic rates of each reaction are given as:

$$r = k\,C_aC_b \rightarrow r = k_{stochastic}N_aN_b, \quad (21)$$

$$k_{stochastic} = k \text{ for monomolecular reaction} \quad (22)$$

$$k_{stochastic} = k/VN_{Avo} \text{ for bimolecular reaction between similar species} \quad (23)$$

$$k_{stochastic} = 2k/VN_{Avo} \text{ for bimolecular reaction between different species} \quad (24)$$

$$r_i = 2k_i\,N_{initiator} \quad (25)$$

$$r_p = 2k_p/VN_{Avo}\,N_LN_M \quad (26)$$

$$r_t = 2k_{tc}/VN_{Avo}\,N_LN_L \quad (27)$$

$$r_{cm} = 2k_{cm}/VN_{Avo}\,N_LN_M \quad (28)$$

$$r_{cp} = 2k_{cp}/VN_{Avo}\,N_LN_D \quad (29)$$

$$r_b = 2k_{beta}/VN_{Avo}\,N_{L_{sec}} \quad (30)$$

The same type of reaction may have different stochastic rates depending on the type of chain. For example, chain transfer to polymer can occur when the target chain is a live or dead polymer. The number of possible radical sites is the total length of all the dead polymer chains when the target chain is a live polymer. Hence, N_D becomes μ_1/λ_0. The number of possible radical sites is the length of the target chain when the target chain is a dead polymer because the target chain receives a radical from the surround-

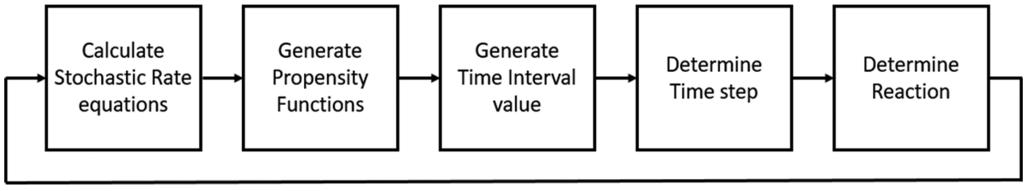

Fig. 3. Flow chart of KMC algorithm proposed by Gillespie.

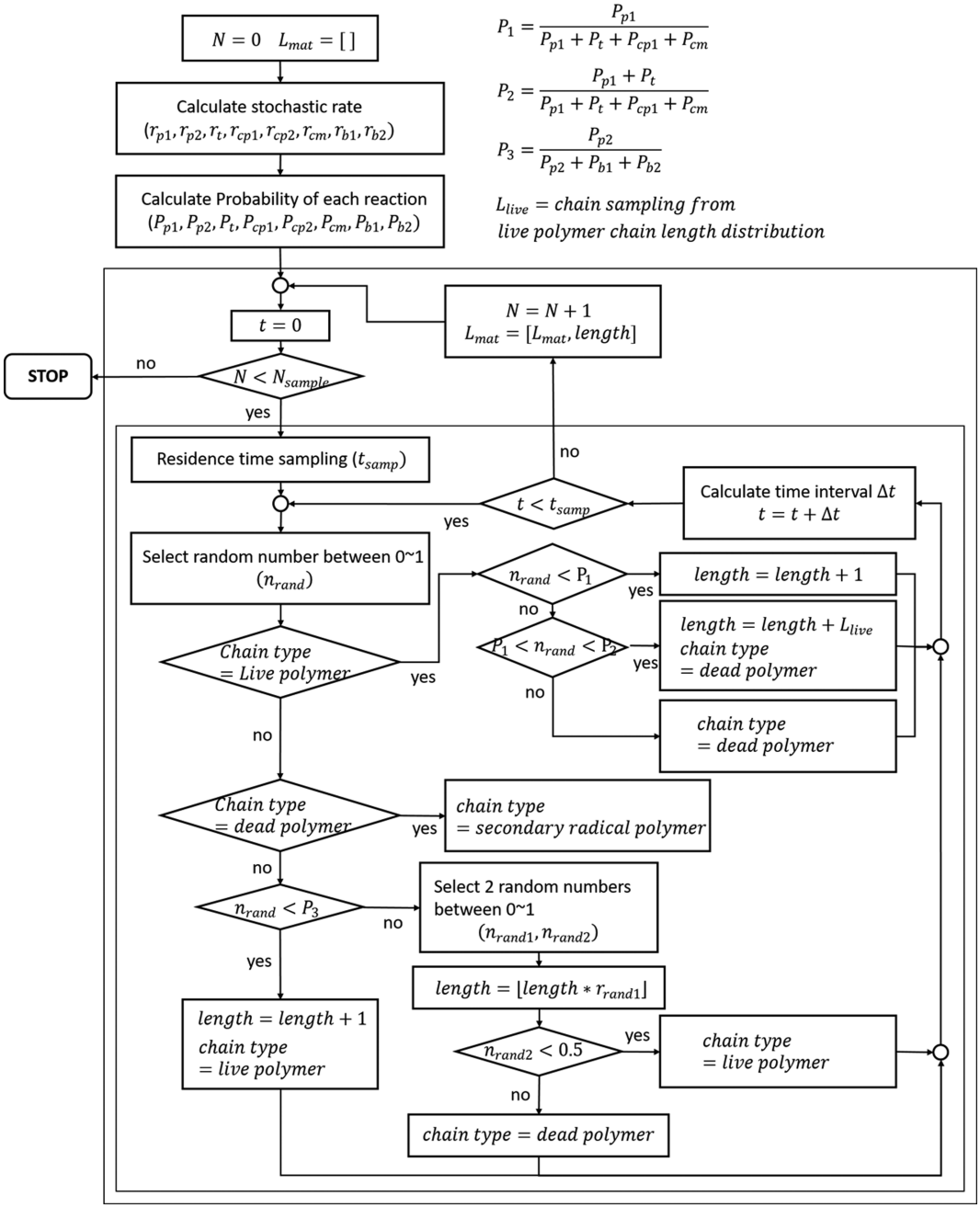

Fig. 4. Flow chart of target chain model.

ing live chain. Therefore, the probability of each reaction is determined, as described in Table 3.

The reaction is determined based on the probabilities with random sampling, and the target chain is updated with this reaction. The only reactions that change the chain length are propagation and termination by combination. In the case of propagation, the length is increased by one, and in the case of termination by combination, the length is increased by the length of the surrounding live polymer. The molecular weight distribution of live polymers is assumed to follow the Schultz-Zimm form, which is the simplest form that can represent a bimodal distribution [36]. Parameters y and h are inversely estimated from [L] and λ_1. Therefore, the live polymer chain that is combined with the target chain is sampled from the Scultz-Zimm distribution of the live polymer chain.

$$\overline{W}(n) = \frac{n^{y}}{h} y^{h} n^{h-1} \exp(-yn)/\Gamma(h) \tag{31}$$

Time interval value is calculated by the reaction rate and random sampling [25].

$$\Delta t = Q_k^{-1} \cdot \ln\left(\frac{1}{n_{rand}}\right) \tag{32}$$

$$Q_{live\ polymer} = R_{p,1} + R_t + R_{cp,1} + R_{cm} \tag{33}$$

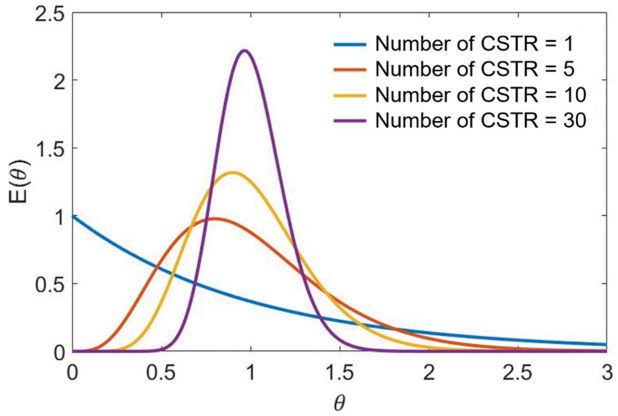

Fig. 5. Residence time distribution according to the number of CSTRs.

$$Q_{dead\ polymer} = R_{cp,2} \quad (34)$$

$$Q_{secondary\ radical\ polymer} = R_{p,2} + R_{beta,1} + R_{beta,2} \quad (35)$$

4-2. Block KMC

The chain grown by the KMC algorithm has a certain pattern in the series of reactions. Because the possible reaction types vary depending on the chain type, seven types of blocks are repeated. These blocks are found by binding the reactions, whose chain type is reverted to the live polymer. The types of blocks and their appearance probabilities are listed in Table 4.

A randomly selected sample from the series of reactions is shown in Fig. 6. These reaction series can be combined into the blocks listed in Table 4.

Each block is independent and the appearance probability is constant. The number of blocks follows a binomial distribution; therefore, it is possible to directly determine the number of blocks in the whole series. The algorithm is shown in Fig. 7.

To determine the number of blocks, we need to know the total number of blocks. However, it is impossible to know the total number of blocks until the end of simulation, because the time interval depends on random numbers. Therefore, we introduce a unit step number to determine the number of blocks. The simulation

Table 3. List of possible reactions depending on the chain type and their probability

Chain type	Possible reaction	Probability
L (Live polymer)	$R_{p,1}$	$P_{p,1} = \frac{r_{p,1}}{r_{p,1} + r_t + r_{cp,1} + r_{cm}}$
	R_t	$P_t = \frac{r_t}{r_{p,1} + r_t + r_{cp,1} + r_{cm}}$
	$R_{cp,1}$	$P_{cp,1} = \frac{r_{cp,1}}{r_{p,1} + r_t + r_{cp,1} + r_{cm}}$
	R_{cm}	$P_{cm} = \frac{r_{cm}}{r_{p,1} + r_t + r_{cp,1} + r_{cm}}$
D (Dead polymer)	$R_{cp,2}$	$P_{cp,2} = 1$
L_{sec} (Secondary radical polymer)	$R_{p,2}$	$P_{p,2} = \frac{r_{p,2}}{r_{p,2} + r_{b,1} + r_{b,2}}$
	$R_{beta,1}$	$P_{b,1} = \frac{r_{b,1}}{r_{p,2} + r_{b,1} + r_{b,2}}$
	$R_{beta,2}$	$P_{p,2} = \frac{r_{b,2}}{r_{p,2} + r_{b,1} + r_{b,2}}$

Table 4. Representation of Blocks and their appearance probabilities

Block	Chain type	Probability
B1) $R_{p,1}$	L→L	$P_{p,1} = \frac{r_{p,1}}{r_{p,1} + r_t + r_{cp,1} + r_{cm}}$
B2-1) $R_t - (R_{cp,2} - R_{beta,2})^n - R_{cp,2} - R_{p,2}$ B2-2) $R_t - (R_{cp,2} - R_{beta,2})^n - R_{cp,2} - R_{beta,1}$	$L \rightarrow (D \rightarrow L_{sec})^n \rightarrow L$	$P_t = \frac{r_t}{r_{p,1} + r_t + r_{cp,1} + r_{cm}}$
B3-1) $R_{cp,1} - (R_{cp,2} - R_{beta,2})^n - R_{cp,2} - R_{p,2}$ B3-2) $R_{cp,2} - R_{cp,2} - R_{beta,2})^n - R_{cp,2} - R_{beta,1}$	$L \rightarrow (D \rightarrow L_{sec})^n \rightarrow L$	$P_{cp,1} = \frac{r_{cp,1}}{r_{p,1} + r_t + r_{cp,1} + r_{cm}}$
B4-1) $R_{cm} - (R_{cp,2} - R_{beta,2})^n - R_{cp,2} - R_{p,2}$ B4-2) $R_{cm} - (R_{cp,2} - R_{beta,2})^n - R_{cp,2} - R_{beta,1}$	$L \rightarrow (D \rightarrow L_{sec})^n \rightarrow L$	$P_{cm} = \frac{r_{cm}}{r_{p,1} + r_t + r_{cp,1} + r_{cm}}$

$$R_{p,1}-R_{p,1}-R_{p,1}-R_{p,1}-R_{p,1}-R_t-R_{cp,2}-R_{beta,2}-R_{cp,2}-R_{beta,2}-R_{cp,2}-R_{p,2}-R_{cm}-R_{cp,2}$$
$$-R_{beta,2}-R_{cp,2}-R_{p,1}-R_{p,1}-R_{p,1}-R_{p,1}-R_{p,1}-R_{p,1}-R_{p,1}-R_{p,1}-R_{p,1}-R_{p,1}-R_{cp,1}-R_{cp,2}$$
$$-R_{beta,2}-R_{cp,2}-R_{beta,2}-R_{cp,2}-R_{beta,2}-R_{cp,2}-R_{beta,2}-R_{cp,2}-R_{beta,2}-R_{cp,2}-R_{beta,1}-\cdots$$

$$\downarrow$$

$$B1-B1-B1-B1-B1-B2_1-B4_2-B1-B1-B1-B1$$
$$-B1-B1-B1-B1-B1-B1-B1-B3_2-\ldots.$$

Fig. 6. Example of reaction series and the series replaced by block.

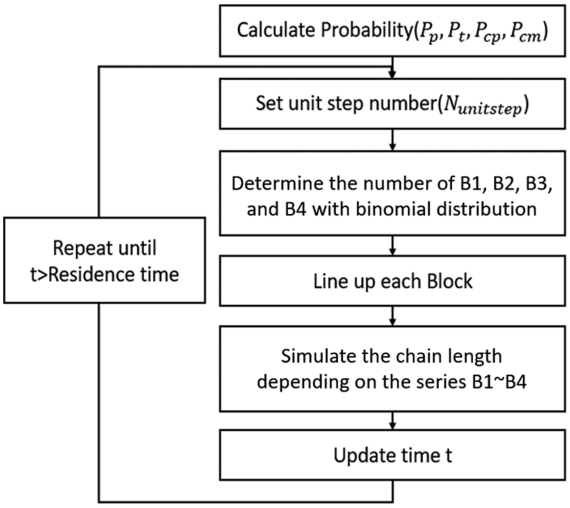

Fig. 7. Flow chart of block KMC algorithm.

is repeated by the unit step number until the time reaches the total residence time of the target chain. In this system, B1 is predominantly selected because the propagation is much faster than other reactions. This means that most of the unit step number is the number of B1 blocks. Because of these features, we can simulate much faster than the conventional MC algorithm.

To calculate the length of the target chain, the number of blocks and the order of blocks must be determined. The algorithm used to set the order of blocks in the target chain model is as follows:

1) Generate $N_{B2}+N_{B3}+N_{B4}+1$ random numbers.

2) Normalize the random numbers so that the sum becomes 1 and multiply each number by N_{B1}.

3) Determine the position of remaining Blocks that will come to the site between the B1 groups based on their probabilities.

Because the number of B1 is much greater than that of the other blocks, the series of blocks takes the form of the remaining blocks between the B1 groups, as presented in Fig. 8. By the first and second stages of the algorithm, we can determine the number of B1 blocks belonging to the B1 groups, which are represented as $n_{i,1}$, $n_{i,2}$, $n_{i,3}$, $n_{i,4}$, … in Fig. 8. In the third stage, the remaining blocks are placed between the B1 groups.

Let us assume that t_1 is the average computation time per step, which consists of random sampling and updating the chain length. The conventional KMC technique requires approximately $N\cdot t_1$ computation time to simulate a total of N reaction series. In the Block KMC model, when the number of propagation reactions is N_p, the first and second stages take $(N-N_p+1)\cdot t_1$, and the third stage takes approximately $(N-N_p)\cdot t_1$ computation time. Hence, the total computation time is approximately $(2*(N-N_p)+1)\cdot t_1$. As expected, because N_p is close to N, $(2\cdot(N-N_p)+1)\cdot t_1$ is much smaller than the computation time of the conventional model $N\cdot t_1$.

RESULT

1. Verification

To verify the Block KMC model, we compared the conventional KMC results with those of the proposed model. These are the results of three different cases by varying the temperature and amount of initiator as indicated in Table 5. The 'Unit Step Number' is fixed at 50.

From the simulation results in Fig. 9, the target model shows over- and under-peaks in the region of small molecular weights. To determine the reason, we classify the chain according to the iteration numbers of the algorithm in Fig. 7. In Fig. 10, the red dotted

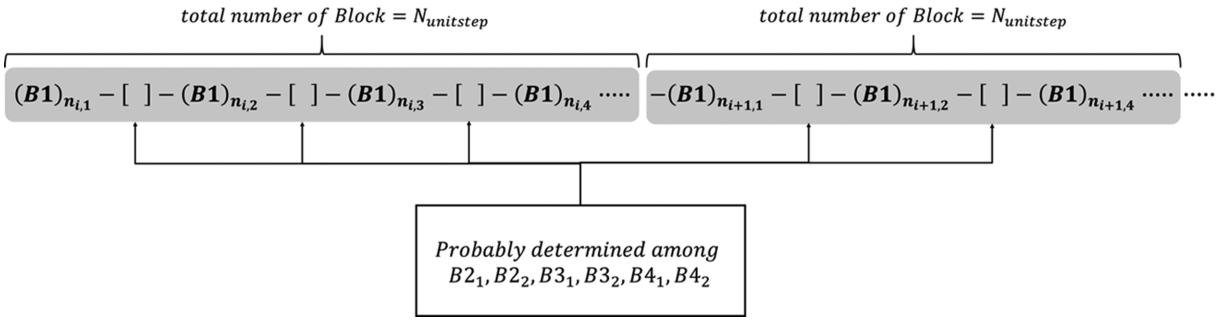

Fig. 8. Representation of block series derived from block KMC method.

Table 5. Operation conditions of Case 1, Case 2, and Case 3

	Case 1	Case 2	Case 3
Temperature (K)	480	490	520
Initiator (mol/L)	10^{-7}	10^{-6}	10^{-7}

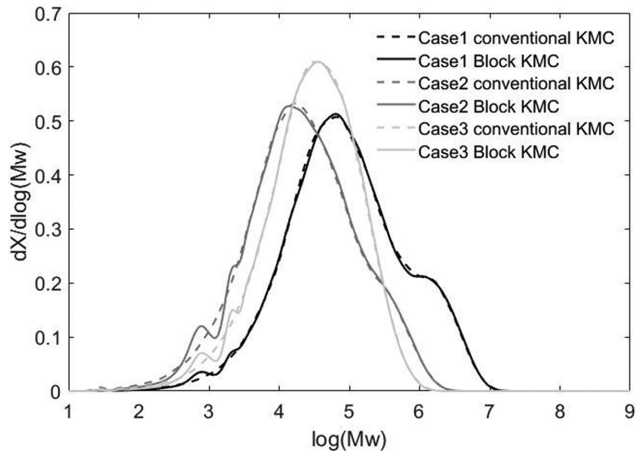

Fig. 9. MWD results from conventional KMC and block KMC models for each case.

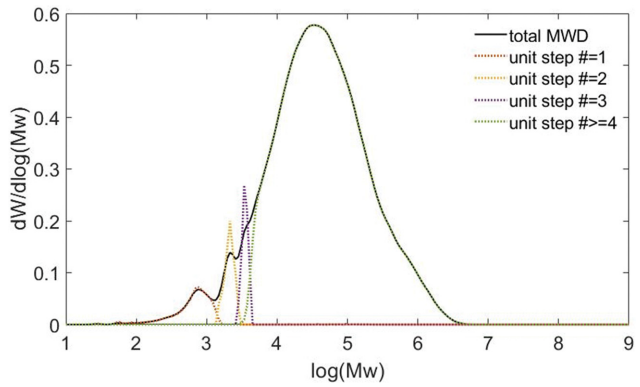

Fig. 10. MWD results depending on iteration number.

line represents the iteration number of 1, the yellow and purple dotted lines represent the MWD when the chain iterates twice and thrice, respectively, and the green dotted line corresponds to the MWD when the chain iterates four or more times. The red, yellow, and purple lines exactly match the point at which the small peaks appear in the entire MWD. This indicates that an error occurs when the number of repetitions is small. This is because the algorithm shows a little oscillation when the total number of Blocks is smaller than the 'Unit Step Number.' The error appears until the number of repetitions is 3 in case the 'Unit Step Number' is 50. To address this issue, when the target chain is short, we set a small 'Unit Step Number' and increase it as the chain length increases. In this way, the model accuracy can be improved while maintaining the calculation time. The detailed setting of the unit step number is shown in Eq. (36). As a result, the modified model removed the small peaks and agreed with the conventional model, as shown in Fig. 11.

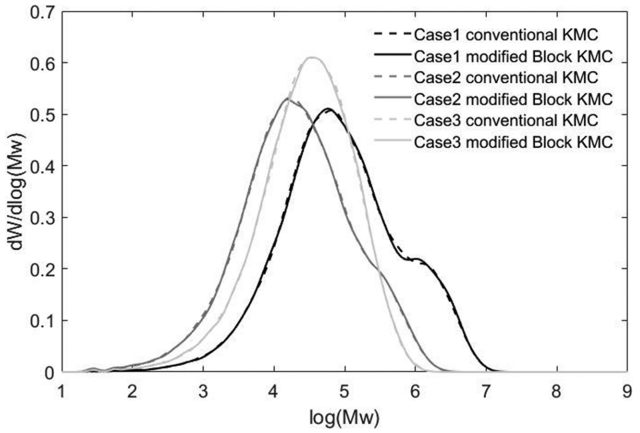

Fig. 11. MWD results of block KMC model in which 'Unit Step Number' is adjusted and compared with traditional KMC model.

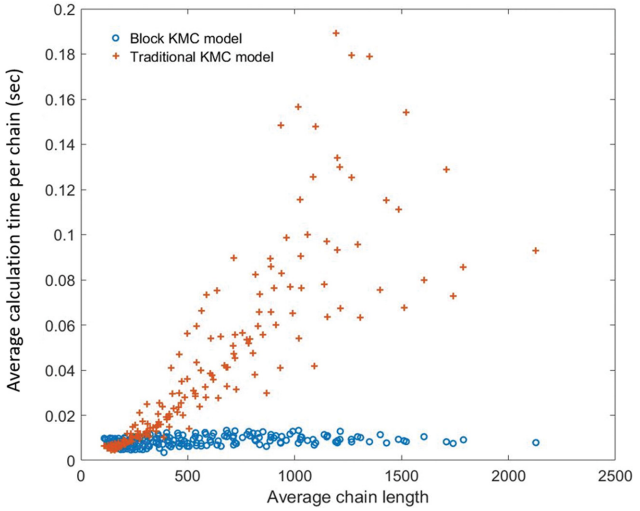

Fig. 12. Average calculation time per one chain according to the average chain length for each model.

$$\begin{cases} \text{Unit step number}=1 & \text{target chain length}<50 \\ \text{Unit step number}=20 & 50\le\text{target chain length}<500 \\ \text{Unit step number}=100 & 500\le\text{target chain length}<5000 \\ \text{Unit step number}=1000 & 5000\le\text{target chain length} \end{cases} \quad (36)$$

2. Reduction in Calculation Time

To quantify the time saved by the proposed model, we measured the average time required to simulate one target chain for each model. Fig. 12 shows the average calculation time per chain according to the chain length. The blue dots are the Block KMC model results, and the red dots are the conventional KMC model results. Although the time difference between the two models is small in the short chain, the Block KMC model becomes much faster in the long chain. As discussed in the Block KMC part in Methodology section, although the conventional method takes $N \cdot t_1$ calculation time, the proposed algorithm only takes $(2 \cdot (N - N_p) + 1) * t_1$.

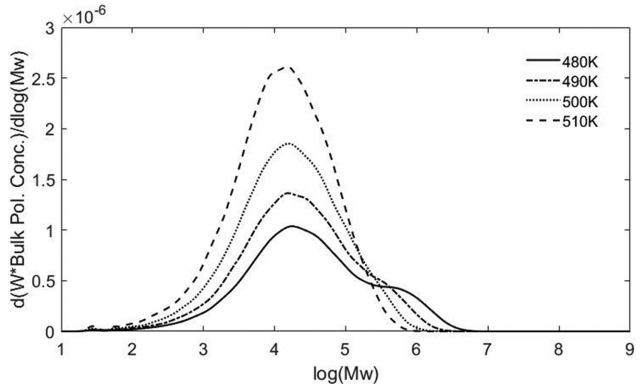

Fig. 13. Effect of temperature on MWD.

This implies that the new algorithm is $1/\left(2\cdot\left(1-\frac{N_p}{N}\right)+\frac{1}{N}\right)$ times faster than the conventional KMC. This is because the unit step number is set much larger in the long chain section. LDPE typically has a molecular weight of less than 50,000 g/mol, which translates to 1,700 mol^{-1} in terms of the number of monomers in the chain. Therefore, at least 10 to 32 times reduction effect can be expected when the chain length is approximately 1700. As shown in Fig. 12, although the calculation time remains constant along the average chain length in the Block KMC model, the calculation time of the conventional method increases in proportion to the average chain length. This indicates that the proposed method has an advantage in simulating polymers with a high Mw.

3. Case Study

Fig. 13 shows the dependence of the molecular weight distribution on the temperature. As the temperature decreases, the formation of the shoulder is observed owing to the generation of more long chains. Calculated properties such as Mn, Mw, PDI and moments according to the temperatures are listed in Table A1. of the Appendix section.

Fig. 14 shows the reaction ratio according to the temperature at various initiator concentrations. The rate ratio of termination to propagation reaction decreases with increasing temperature because the kinetic constant of termination is less sensitive to temperature as indicated in Table 6, and the live polymer concentration decreases as the temperature increases.

$$\frac{R_t}{R_p}=\frac{k_t\lambda_0^2}{k_p\lambda_0[M]}=\frac{k_t\lambda_0}{k_p[M]} \tag{37}$$

The rate ratio of the chain transfer to polymer to propagation increases as the temperature increases. This is because the kinetic constant of the chain transfer to polymer reactions is more sensitive, and the dead polymer weight concentration increases with temperature.

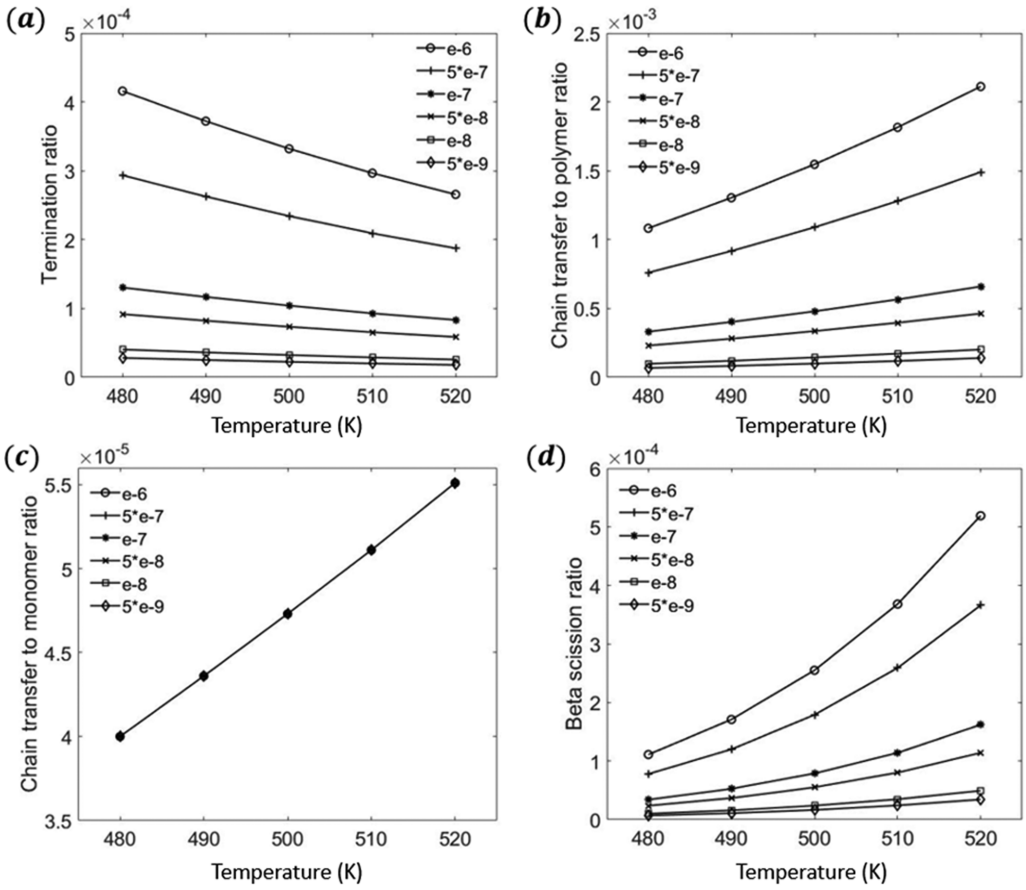

Fig. 14. Reaction ratio according to temperature at various initiator concentrations (a) R_t/R_p, (b) R_{cp}/R_p, (c) R_{cm}/R_p, and (d) R_b/R_p.

Table 6. Temperature sensitivity of reaction mechanism

Reaction mechanism	Activation energy J/mol	Temperature sensitivity
Initiation decomposition	149,347	Highest
Beta scission	83,997	
Chain transfer to polymer	46,369	
Chain transfer to monomer	37,802	
Propagation	29,783	
Termination	10,080	Lowest

$$\frac{R_{cp}}{R_p}=\frac{k_{cp}\lambda_0\mu_1}{k_p\lambda_0[M]}=\frac{k_{cp}\mu_1}{k_p[M]} \tag{38}$$

The rate ratio of beta scission to propagation increases as the temperature increases. This is because the kinetic constant of the beta scission is more sensitive, and the secondary radical concentration increases with temperature, while the live polymer concentration decreases.

$$\frac{R_b}{R_p}=\frac{k_b\lambda_{sec,0}}{k_p\lambda_0[M]} \tag{39}$$

The rate ratio of chain transfer to monomer increases as the temperature increases because the rate constant of the chain transfer to monomer is more sensitive to temperature, and the ratio is constant even if the concentration changes.

$$\frac{R_{cm}}{R_p}=\frac{k_{cm}\lambda_0[M]}{k_p\lambda_0[M]}=\frac{k_{cm}}{k_p} \tag{40}$$

The results of MWD according to the temperature can be interpreted by the ratio results of each reaction. MWD becomes narrower as the ratio of the chain transfer to polymer to the propagation

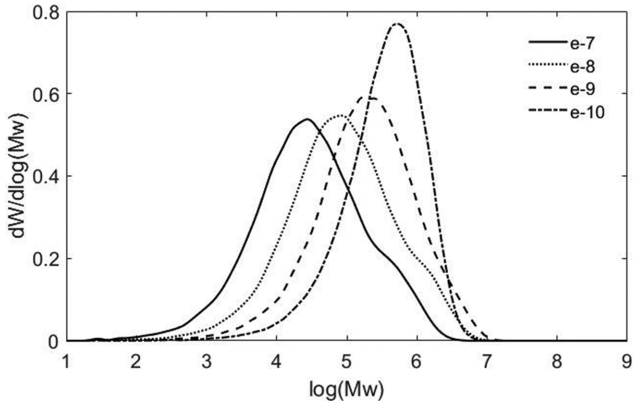

Fig. 15. Effect of initiator concentration on MWD.

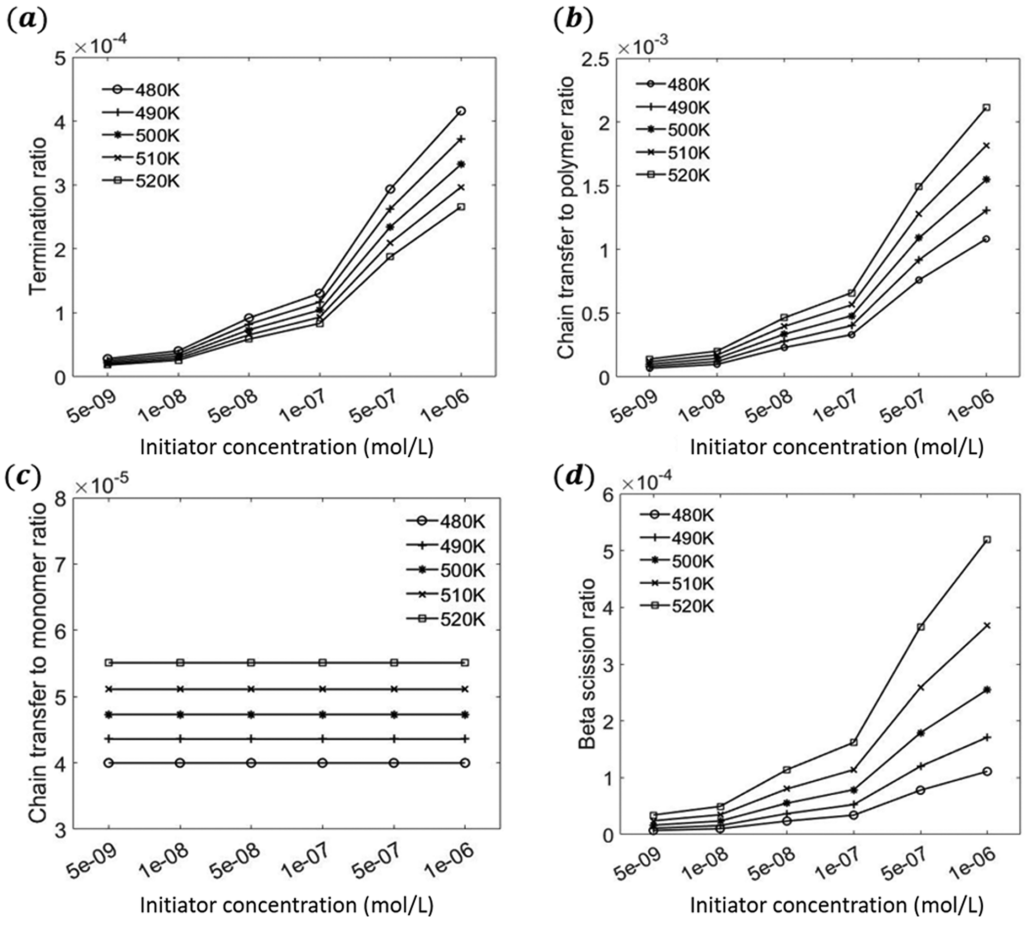

Fig. 16. Reaction ratio according to initiator concentration at various temperatures (a) R_t/R_p, (b) R_{cp}/R_p, (c) R_{cm}/R_p, and (d) R_b/R_p.

increases with increasing temperature. This does not agree with the fact that the chain transfer to polymer broadens MWD. This means that the broadness of MWD is not determined only by the chain transfer to polymer, but also by the termination and beta scission. At low temperatures, as the termination reaction becomes dominant, the chains are combined to increase the proportion of long chains. At high temperatures, the beta scission predominates, and occurs better than the propagation in the secondary radical chain generated from the chain transfer to polymer. Therefore, the chain does not become a higher branched chain but breaks into smaller chains, which causes the left shift of MWD.

Fig. 15 shows the dependence of the molecular weight distribution on the initiator concentration. As the initiator concentration increases, the formation of the shoulder is observed and the average chain length decreases. Calculated properties such as Mn, Mw, PDI and moments according to the initiator concentration are listed in Table A2 of the Appendix section.

Fig. 16 shows the reaction ratio according to the initiator concentrations at various temperature. The rate ratio of termination to propagation increases with increasing initiator concentration because the live polymer concentration increases as the initiator concentration increases. The rate ratio of the chain transfer to polymer to propagation also increases as the initiator concentration increases, because the dead polymer weight concentration increases as the initiator concentration increases. The rate ratio of beta scission to propagation increases as the temperature increases because the secondary radical concentration increases faster than the live polymer concentration. The rate ratio of the chain transfer to monomer is constant as the initiator concentration increases because the rate constant of the chain transfer to monomer does not depend on the concentration.

As the initiator concentration decreases, the MWD becomes narrower and shifts to the right. The plot shows a broad distribution because both long and short chains are produced as the termination and beta scission become faster. In addition, because the termination is more dominant than the beta scission under a low initiator concentration, the distribution plot moves to the right and the values of Mn and Mw also increase.

4. Shouldering Condition

Because each reaction affects the MWD in a complex manner, it is impossible to determine the condition in which a shoulder of the MWD is generated by only one reaction. Therefore, 180 cases were simulated by varying the temperature, initiator amount, and average residence time to determine the condition of the shoulder appearing. The range of operation conditions is listed in Table 7. In Fig. 17, each reaction ratio is set as an axis. Blue and red dots represent the shouldered and non-shouldered cases, respectively. To formulate the reaction conditions in which the shoulders are generated, a flat plane is found that separates the blue and red dots

Table 7. Range of operation condition

Operation condition	Range
Temperature	480-520 K
Initiator concentration	$5*10^{-9}$-10^{-6} mol/L
Average residence time	10-60 sec

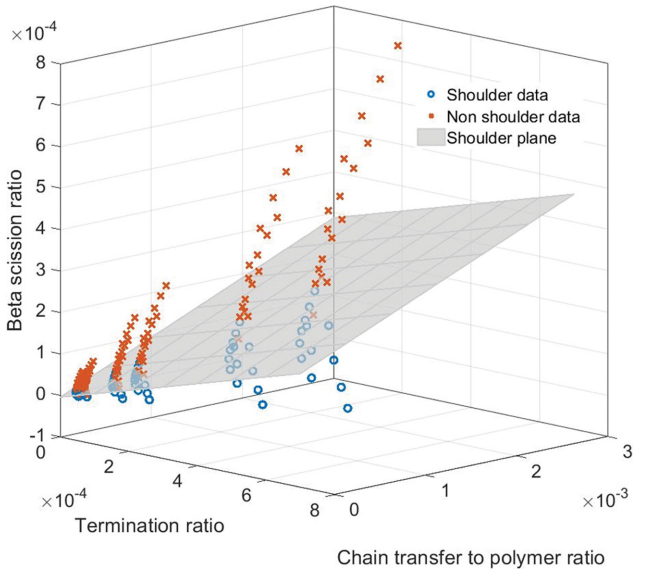

Fig. 17. Shoulder plane for LDPE in CSTR reactor (F_{sh}=0 from Eq. (41)).

through a linear support vector machine (SVM) technique. The hyperplane equation is given by Eq. (41), and the model classification accuracy is 89%.

$$F_{sh}=-0.585\phi_t-0.223\phi_{cp}+2.286\phi_{beta}+0.6*10^{-5} \quad (41)$$

ϕ_t=Rate ratio of termination to propagation, R_t/R_p
ϕ_{cp}=Rate ratio of the chain transfer to polymer to propagation, R_{cp}/R_p
ϕ_{beta}=Rate ratio of beta scission to propagation, R_{beta}/R_p

if $F_{sh}>0$, nonshouldered MWD (42)
else $F_{sh}<0$, shouldered MWD

Under the condition that the F_{sh} value is positive, MWD does not have a shoulder. When F_{sh} is negative, the MWD has a shoulder. The faster the termination and the chain transfer to polymer and the slower the beta scission, the higher the probability that MWD will have a shoulder, which is consistent with a previous study [12,19,32,38]. As discussed in the case study on temperature, it is confirmed that the shoulder can be generated by the termination and beta scission, despite the decrease in the chain transfer to polymer reaction ratio.

CONCLUSION

We have proposed an MWD prediction model that couples deterministic and stochastic methods. We introduced a new concept of 'Block,' which is a group of repeating reaction series. It reveals that the model is approximately 10 to 32 times faster than the model proposed by Neuhaus [30], with almost the same performance. There are two reasons for the model to reduce the computation time effectively. First, the number of blocks follows a binomial distribution, which makes it possible to determine each reaction quickly. Second, since the propagation is much faster than other reactions, the model can effectively reduce the calculation time for ordering the reactions. This reveals that the larger the average molecular

weight of the polymer, the greater is the time reduction effect. Therefore, the model can be effectively applied to HDPE or higher-molecular-weight polymers.

We simulated the MWD and calculated the rate ratio of other reactions to the propagation according to the temperature and initiator concentration. The MWD was finally determined as the kinetic effects of each reaction that interact with each other. Some studies have dealt with the effects of operation conditions [12,39,40], but it is still challenging to analyze how the reactions comprehensively affect the MWD. In particular, the shouldering phenomenon remains a poorly understood topic, as it does not necessarily correlate with the average molecular weight. This makes it difficult to obtain the desired product, while making the operation of the reaction system difficult. Therefore, in this study, we provided a quantitative guideline for the appearance of the shoulder with 89% accuracy by simulating 180 cases for the operating conditions shown in Table 7.

The model was developed using a CSTR reactor. For a practical reactor, the viscosity of the fluid in the reactor increases as the polymerization proceeds, hindering perfect mixing and heat transfer. Furthermore, the reaction system was controlled with several input flows by regulating the temperature or initiator concentration. Therefore, industrial polymer reactors exhibit inhomogeneous behavior. The conventional KMC technique takes too long to combine with the flow data, whereas the proposed model is applicable because of its reduced computation time. Therefore, the proposed model can be applied to an industrial-scale reactor for real-time control and optimization.

ACKNOWLEDGEMENTS

This work was supported by the National Research Foundation of Korea (NRF) grant funded by the Korea government (MSIT) (No. 2020R1A2C1005503).

NOTATIONS

C_a : concentration of molecule a [mol/L]
D_n : dead polymer chain of length n
f : effectiveness factor for initiator decomposition [dimensionless]
F_{sh} : shouldering measurement [dimensionless]
k : kinetic constant
k_b : kinetic constant of beta scission reaction [s^{-1}]
k_{cp} : kinetic constant of chain transfer to polymer reaction [$L(mol \cdot s)^{-1}$]
k_{cm} : kinetic constant of chain transfer to monomer reaction [$L(mol \cdot s)^{-1}$]
k_d : kinetic constant of initiator decomposition reaction [s^{-1}]
k_p : kinetic constant of propagation reaction[$L(mol \cdot s)^{-1}$]
k_t : kinetic constant of termination by combination reaction [$L(mol \cdot s)^{-1}$]
L_n : live polymer chain of length n
$L_{n,sec}$: secondary radical polymer chain of length n
L_{live} : chain length sampled from the live polymer chain length distribution
L_{mat} : the matrix where chain length data is stored
M : ethylene monomer
N : number of simulated taget chain
N_a : number of molecules
N_{AVO} : Avogadro number
N_{B1} : number of B1 blocks
N_{B2} : number of B2-1 and B2-2 blocks
N_{B3} : number of B3-1 and B3-2 blocks
N_{B4} : number of B4-1 and B4-2 blocks
n_{rand} : random number between 0-1
N_{samp} : total number of taget chains to be simulated
P_{p1}, P_{p2} : Probabilities of propagation reaction
P_t : Probabilities of termination by combination reaction
P_{cp1}, P_{cp2} : Probabilities of chain transfer to polymer reaction
P_{cm} : Probabilities of chain transfer to monomer reaction
P_{b1}, P_{b2} : Probabilities of beta scission reaction
r : stochastic reaction rate
R_i : initiator decomposition reaction
R_{p1}, R_{p2} : propagation reaction
R_t : termination by combination reaction
R_{cp1}, R_{cp2} : chain transfer to polymer reaction
R_{cm} : chain transfer to monomer reaction
R_{beta1}, R_{beta2} : beta scission reaction
r_{p1}, r_{p2} : stochastic rate of propagation reaction [$mol \cdot s^{-1}$]
r_t : stochastic rate of termination by combination reaction [$mol \cdot s^{-1}$]
r_{cp1}, r_{cp2} : stochastic rate of chain transfer to polymer reaction [$mol \cdot s^{-1}$]
r_{cm} : stochastic rate of chain transfer to monomer reaction [$mol \cdot s^{-1}$]
r_{b1}, r_{b2} : stochastic rate of beta scission reaction [$mol \cdot s^{-1}$]
T : average residence time in CSTR reactor [sec]
t : current simulation time [sec]
t_{samp} : residence time of target chain [sec]
V : total volume of reactor system [L]
v : volumetric flow rate of input flow [L/s]
[D] : concentration of dead polymer [mol/L]
$[D_n]$: concentration of the dead polymer of length n [mol/L]
[I] : concentration of initiator [mol/L]
[L] : concentration of live polymer [mol/L]
$[L_n]$: concentration of the live polymer of length n [mol/L]
$[L_{sec}]$: concentration of secondary radical polymer [mol/L]
$[L_{sec,n}]$: concentration of the secondary radical polymer of length n [mol/L]
[M] : concentration of monomer [mol/L]
λ_k : k^{th} moment of live polymer chain
$\lambda_{sec,k}$: k^{th} moment of secondary radical polymer chain
μ_k : k^{th} moment of dead polymer chain

REFERENCES

1. F. A. Bovey, F. C. Schilling, F. L. McCrackin and H. L. Wagner, *Macromolecules*, **9**, 76 (1976).
2. J. K. Beasley, *J. Am. Chem. Soc.*, **75**, 6123 (1953).
3. W. H. Ray, *J. Macromol. Sci., Rev. Macromol. Chem.*, **8**, 1 (1972).
4. T. J. Crowley and K. Y. Choi, *Ind. Eng. Chem. Res.*, **36**, 1419 (1997).

5. P. D. Iedema, M. Wulkow and H. C. Hoefsloot, *Macromolecules*, **33**, 7173 (2000).
6. S. H. Son, J. J. Han and J. M. Lee, *Polymer*, **126**, 74 (2017).
7. B. M. Louie, G. M. Carratt and D. S. Soong, *J. Appl. Polym. Sci.*, **30**, 3985 (1985).
8. A. G. Mikos, C. G. Takoudis and N. A. Peppas, *Macromolecules*, **19**, 2174 (1986).
9. S. Zhu and A. E. Hamielec, *Macromolecules*, **22**, 3093 (1989).
10. S. Zhu and A. E. Hamielec, *J. Polym. Sci. Part B: Polym. Phys.*, **32**, 929 (1994).
11. S. Shin, S. Choi, J. Na, I. Jung, M.-K. Kim, M.-J. Park and W. B. Lee, *Chem. Eng. J.*, 131829, https://doi.org/10.1016/j.cej.2021.131829.
12. G. J. Wells and W. H. Ray, *Macromol. Mater. Eng.*, **290**, 319 (2005).
13. P. Pladis and C. A. Kiparissides, *Chem. Eng. Sci.*, **53**, 3315 (1998).
14. R. A. Hutchinson, *Macromol. Theory Simul.*, **10**, 144 (2001).
15. S. X. Zhang and W. H. Ray, *AIChE J.*, **43**, 1265 (1997).
16. H. Tobita, *J. Polym. Sci., Part B: Polym. Phys.*, **39**, 391 (2001).
17. N. Yaghini and P. D. Iedema, *Chem. Eng. Sci.*, **116**, 144 (2014).
18. D. Meimaroglou, P. Pladis, A. Baltsas and C. Kiparissides, *Chem. Eng. Sci.*, **66**, 1685 (2011).
19. D. M. Kim, M. Busch, H. C. Hoefsloot and P. D. Iedema, *Chem. Eng. Sci.*, **59**, 699 (2004).
20. C. Kiparissides, A. Krallis, D. Meimaroglou, P. Pladis and A. Baltsas, *Chem. Eng. Technol.*, **33**, 1754 (2010).
21. P. D. Iedema and H. C. Hoefsloot, *Macromol. Theory Simul.*, **10**, 855 (2001).
22. D. M. Kim and P. D. Iedema, *Chem. Eng. Sci.*, **59**, 2039 (2004).
23. D. M. Kim and P. D. Iedema, *Chem. Eng. Sci.*, **63**, 2035 (2008).
24. N. Yaghini and P. D. Iedema, *Chem. Eng. Sci.*, **130**, 310 (2015).
25. D. T. Gillespie, *J. Phys. Chem.*, **81**, 2340 (1977).
26. H. Tobita, *Macromol. Theory Simul.*, **5**, 129 (1996).
27. H. Tobita, *Macromol. React. Eng.*, **7**, 181 (2013).
28. H. Tobita, *Macromol. Theory Simul.*, **23**, 182 (2014).
29. M. Rogošić, H. J. Mencer and Z. Gomzi, *Eur. Polym. J.*, **32**, 1337 (1996).
30. E. Neuhaus, T. Herrmann, I. Vittorias, D. Lilge, G. Mannebach, A. Gonioukh and M. Busch, *Macromol. Theory Simul.*, **23**, 415 (2014).
31. C. Schütte and M. Wulkow, *Macromol. React. Eng.*, **4**, 562 (2010).
32. D. Eckes and M. Busch, *Macromol. Symp.*, **360**, 23 (2016).
33. D. Meimaroglou and C. A. Kiparissides, *Macromolecules*, **43**, 5820 (2010).
34. P. Feucht, B. Tilger and G. Luft, *Chem. Eng. Sci.*, **40**, 1935 (1985).
35. H. Tobita, *Processes*, **3**, 731 (2015).
36. I. L. Chien, T. W. Kan and B. S. Chen, *Comput. Chem. Eng.*, **31**, 233 (2007).
37. A. M. Kotliar, *J. Polym. Sci., Part A: Gen. Pap.*, **2**, 4303 (1964).
38. A. Krallis, P. Pladis and C. Kiparissides, *Macromol. Theory Simul.*, **16**, 593 (2007).
39. N. H. Kolhapure and R. O. Fox, *Chem. Eng. Sci.*, **54**, 3233 (1999).
40. L. Marini and C. Georgakis, *Chem. Eng. Commun.*, **30**, 361 (1984).

APPENDIX

Table A1. Calculated properties of products at various temperatures

Temperature	Mn	Mw	PDI	μ_1, mol/L	λ_0, mol/L	$\lambda_{sec,0}$, mol/L
480 K	$1.81*10^5$	$1.13*10^6$	6.23	0.0022	$1.15*10^{-8}$	$1.11*10^{-11}$
490 K	$9.24*10^4$	$5.19*10^5$	5.62	0.0026	$1.13*10^{-8}$	$1.29*10^{-11}$
500 K	$5.32*10^4$	$2.46*10^5$	4.63	0.0029	$1.11*10^{-8}$	$1.44*10^{-11}$
510 K	$3.5*10^4$	$1.36*10^5$	3.89	0.0033	$1.09*10^{-8}$	$1.58*10^{-11}$

Table A2. Calculated properties of products at various initiator concentrations

Initiator concentration	Mn	Mw	PDI	μ_1, mol/L	λ_0, mol/L	$\lambda_{sec,0}$, mol/L
$5*10^{-7}$	$1.27*10^5$	$6.97*10^5$	5.51	$1.80*10^{-3}$	$8.01*10^{-9}$	$6.39*10^{-12}$
$5*10^{-8}$	$3.35*10^5$	$1.67*10^6$	5.14	$5.55*10^{-4}$	$2.51*10^{-9}$	$6.12*10^{-13}$
$5*10^{-9}$	$5.67*10^5$	$2.36*10^6$	4.17	$1.64*10^{-4}$	$7.72*10^{-10}$	$5.57*10^{-14}$
10^{-10}	$6.34*10^5$	$1.39*10^6$	2.19	$1.78*10^{-5}$	$8.53*10^{-11}$	$6.54*10^{-16}$

ABBREVIATIONS

CSTR : continuous stirred-tank reactor
CTA : chain transfer agent
HDPE : high density polyethylene
KMC : kinetic monte carlo
LDPE : low density polyethylene
MC : monte carlo
MI : melt index
MoM : method of moment
MWD : molecular weight distribution
PDI : polydispersity index
SMMA : single macromolecule approach
SVM : support vector machine